Targeting STAT3 anti-apoptosis pathways with organic and hybrid organic–inorganic inhibitors

Matthew B. Minus[4], **Haopei Wang**[1], **Jaime O. Munoz**[2], **Alexandra M. Stevens**[2], **Alicia E. Mangubat-Medina**[1], **Michael J. Krueger**[2], **Wei Liu**[2], **Moses M. Kasembeli**[3], **Julian C. Cooper**[1], **Mikhail I. Kolosov**[5], **David J. Tweardy**[3,6], **Michele S. Redell**[2], **Zachary T. Ball**[1,*]

[1]Department of Chemistry, Rice University, Houston, TX 77005 (USA).

[2]Baylor College of Medicine, Texas Children's Cancer Center, Houston, TX 77030 (USA).

[3]Department of Infectious Diseases, Infection Control and Employee Health, The University of Texas MD Anderson Cancer Center, Houston, TX 77030 (USA).

[4]Prairieview A&M University, Prairie View, TX, 77446 (USA)

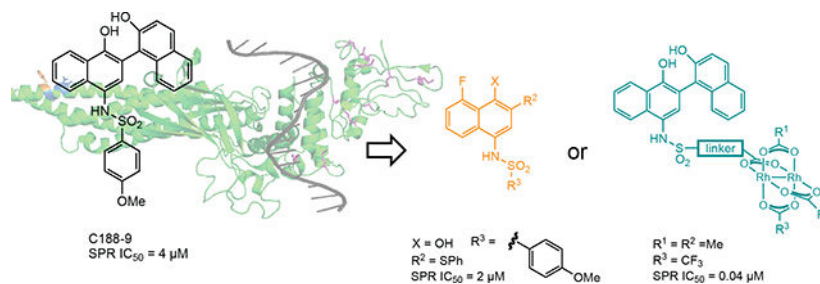[5]Department of Medicine, Baylor College of Medicine, Houston, TX 77030 (USA)

[6]Department of Molecule and Cellular Oncology, The University of Texas MD Anderson Cancer Center, Houston, TX 77030 (USA).

Abstract

Recurrence and drug resistance are major challenges in the treatment of acute myeloid leukemia (AML) that spur efforts to identify new clinical targets and active agents. STAT3 has emerged as a potential target in resistant AML, but inhibiting STAT3 function has proven challenging. This paper describes synthetic studies and biological assays for a naphthalene sulfonamide inhibitor class of molecules that inhibit G-CSF-induced STAT3 phosphorylation in cellulo and induce apoptosis in AML cells. We describe two different approaches to inhibitor design: First, variation of substituents on the naphthalene sulfonamide core allows improvements in anti-STAT activity and creates a more thorough understanding of anti-STAT SAR. Second, a novel approach involving hybrid sulfonamide–rhodium(II) conjugates tests our ability to use cooperative organic–inorganic binding for drug development, and to use SAR studies to inform metal conjugate design. Both approaches have produced compounds with improved binding potency. In vivo and in cellulo experiments further demonstrate that these approaches can also lead to improved activity in living cells, and that compound **3aa** slows disease progression in a xenograft model of AML.

Graphical Abstract

---

*Corresponding Author.

C188-9
SPR IC$_{50}$ = 4 μM

X = OH   R^3 =
R^2 = SPh
SPR IC$_{50}$ = 2 μM

R^1 = R^2 =Me
R^3 = CF$_3$
SPR IC$_{50}$ = 0.04 μM

Keywords

STAT3; Leukemia; naphthylsulfonamide; iminonaphthoquinone

Introduction

Signal transducer and activator of transcription (STAT) proteins are intracellular signaling proteins that mediate response to extracellular stimuli.[1–3] Extracellular signaling proteins, such as cytokines and growth factors, activate membrane-bound receptors that then recruit and tyrosine phosphorylate the STAT3 loop domain immediately C-terminal to the SH2 domain.[4] Phosphorylated STAT3 (pSTAT3) dimerizes and translocates to the nucleus where it activates transcription of tumor survival pathways.[5,6] The aberrant activation of STAT3 is a common occurrence in many cancers.[6,7] Inhibition of STAT3 activity has been shown to lead to apoptosis in cancers such as breast,[8,9] head and neck,[10,11] colon,[12] liver,[13] acute myeloid leukemia (AML),[14,15] and prostate.[16] Thus, STAT3 has been implicated as a promising protein target for the development of broad-spectrum chemotherapeutics.[17]

In spite of significant efforts, inhibiting STAT3 pathways has proven difficult.[18] Blocking intracellular protein–protein interactions like those that mediate STAT3 activation remains a daunting pharmacological goal.[19,20] We became interested in naphthalene sulfonamides as anti-STAT3 compounds,[4,11,14,21] and sought to understand the molecular basis of STAT3 binding, to identify their molecular target on STAT3, and to assess the anti-AML activity of these compounds in molecular, cellular, and animal models of AML. We began this exploration assuming that the lead compound, C188–9 (a.k.a. TTI-101) (Figure 1b), competitively binds to the phosphotyrosine peptide binding site in SH2 domain, consistent with previous assumptions (Figure 1a). During the course of our investigations, rhodium-catalyzed proximity-driven covalent modification determined that modified naphthalene sulfonamides also target a new binding site in the coiled-coil domain (CCD), and that, importantly, binding to this site is not competed by the natural phosphotyrosine peptide (Figure 1a, orange residue).[15] In part, current research seeks to investigate the therapeutic potential of targeting CCD.[15]

At the same time, the challenges of STAT3 inhibition provided an opportunity to explore an unconventional approach to inhibitor development: employing rhodium–small molecule conjugates as anti-STAT agents. Conceptually, the approach is based on cooperative organic–inorganic binding that includes rhodium coordination to a Lewis-basic side chain near protein binding interface (Figure 1c).[22,23] We have demonstrated this concept with

rhodium-peptide conjugates, and this work provided an opportunity to explore the concept with non-peptide inhibitors (Figure 1c). Cellular studies provided an opportunity to assess function in living cells, as opposed to purely biophysical measurements, and these measurements shed light on the benefits and limitations of rhodium-based approaches, compared to traditional small-molecule STAT3 inhibitors.

Inhibitor Synthesis

Naphthalene sulfonamides were identified as lead fragments through a combination of screening and limited structural variation.[21] Compounds with STAT3-binding activity permit significant variation of the sulfonamide substituent (R^3 in), thus R^3 was seen as the most straightforward site for incorporation of rhodium centers, via target structures such as **13aa-13c**. Furthermore, the C5–C8 positions of the naphthalene ring (R^4) were a largely unexplored site of variation. In the course of our studies, we became further interested in variation of the naphthol, and in assessing the function of redox variants of this core, such as the iminoquinone.

In the synthetic direction, the requisite 2-substituted naphthalene sulfonamides (e.g. **2a–4d**, Scheme 1) are readily available via elaboration of simple naphthalene sulfonamides (**1a–1f**, Scheme 1) after sulfonamide formation from 4-amino-1-naphthol. Formation of the sulfonamide early in the synthesis is important to limit synthetic manipulations with oxidatively sensitive free 4-amino-1-naphthol derivatives. Elaboration of the 2-position of the naphthalene ring with halogens is directly achieved by electrophilic aromatic substitution to afford arylbromides (**2a-2c**). Alternatively, oxidative coupling with pro-nucleophiles (Nu–H = Ar–H, RS–H, RO–H) succeeds via the intermediacy of an iminobenzoquinone **1a^ox-1f^ox**.[25] This allowed preparation of a variety of additional S-linked (**3aa-3cd**) and C-linked (**4a-4d**) 2-substitution products.

In tandem, we set our sights on 8-substituted derivatives that could provide electronic and steric perturbation of the naphthalene core, both to investigate SAR in this region and to perturb the redox stability of inhibitor molecules. In a first approach, (Scheme 2), we synthesized 1,8-difluoronaphthalene from 1,8-diaminonaphthalene,[26] via a bis-diazonium intermediate. The 1,8-difluoronaphthalene was nitrated at the 4-position (**5**), and nucleophilic aromatic substitution of the fluorine para to nitro with an alkoxide delivered naphthyl ether, and subsequent hydrogenolysis yield **7**. Efforts in this direction were limited by safety and scalability concerns: The bis-diazonium salt was prone to spontaneous and at times violent decomposition. As an alternative, we exploited more recent advances[27] in nucleophilic aromatic fluorination to prepare **6** from 1,5-dinitronaphthalene (Scheme 2). This route gave better access to fluorinated naphthalene intermediates. The electrophilic naphthalene ring **6** could be oxidized with *tert*-butylhydroperoxide (TBHP) in liquid ammonia to install a hydroxyl group, affording naphthol **7**. Etherification of the OH group was next performed, providing a benzyl (**8**) or methyl (**10**) ether. At this point, the nitro group could be reduced selectively in the presence of a platinum catalyst, and the resulting aniline then coupled with a sulfonyl chloride to provide sulfonamide **8**. Deprotection of the benzyl group and oxidative coupling with thiophenol gave fluoride **9**. Alternatively, the methyl ethers **12a** and **12b** were synthesized as analogues of compounds **2a-2c**.

Several structures with different ester functional groups serve as anchor points for rhodium conjugation (**4a, 4b, 4c** in Table 1). General methods that have been previously reported allow for facile cooperative rhodium(II) binding to neighboring residues that strongly coordinate to metal centers, such as methionine or histidine, allowed 50–500 fold increases in potency in other systems.[23,24,28] The presumptive target of naphthalene sulfonamide inhibitors, the SH2 domain, contained several such residues (Figure 1a, purple). However, the coiled coil domain—later identified as another target of naphthalene sulfonamide inhibitors—is devoid of histidine, cysteine, and methionine residues. This discovery allowed us to assess the suitability of cooperative inhibition with rhodium conjugates toward binding sites that lack such strong metal-binding sites. (Figure 1a, blue). We chose to append esters onto the C4 substituent of the naphthalene ring (), a region of the inhibitor which was previously found to be tolerant to steric and electronic variations.[21] We prepared several rhodium conjugates from ester-containing intermediates by acidic hydrolysis followed by metalation with a heteroleptic rhodium reagent containing labile trifluoroacetate groups (Table 2). Unfortunately, Rh-naphthylsulfonamide conjugates could not be made by traditional procedures that involve refluxing the carboxylate inhibitors in benzene. These conditions proved to be too harsh for the organic starting materials. Instead methodologies previously developed by our group were used to successfully couple these small molecules to rhodium.15

SPR analysis

Potency was initially assessed by surface plasmon resonance (SPR), allowing quantification of binding and straightforward comparison to other studies.[21] Variation of the R^1 and R^2 groups provided additional insight into the structural landscape of affinity. A perfluorinated ring within compound **2a**—suggested by the appearance of this group in another STAT-binding compound,[8,29] results in a 3-fold increase in potency from **C188–46** (Table 2). When this change was combined with variation at the C2 position, significant gains in affinity were observed. Compound **3aa** was found to be 10-fold more potent than **2a**. Being inspired by this increase in potency, we made different analogues of the inhibitors. In general inhibitors with thiophenyl in the C2 position displayed greater potency. Even when the perfluorinate ring in the R1 position was replaced with another alkyl or aryl group, the potency remained similar. In addition, it seems the thiophenyl ring is functionally tolerant to hydroxylation and alkylation. Inhibitors (**3cb-3cd**) were only slightly less potent than their parent compound (**3ca**). In summary, SPR analysis demonstrates that molecular recognition of the inhibitor to STAT3 is dependent on the 1,2,4 substitution on the naphthalene ring. This is highlighted by the fact that smaller molecules without the sulfonamide-like moiety (**14–16**) still inhibit STAT3-phosphopeptide binding.

Naphthalene sulfonamide oxidation

The 1,4-substitution pattern of hydroxyl-naphthalenesulfonamides renders the core structure susceptible to oxidation. Some synthetic intermediates (i.e. **1b**, **1c**, and **1f**) indeed proved quite prone to air oxidation and subsequent decomposition. *In vivo* oxidation could be a decomposition pathway, but it is also possible that oxidized iminoquinone species (e.g. Table 2, 2b*) may represented an active species, with naphthalenesulfonamides serving as a pro-

drug. Iminoquinone structures might serve as reactive electrophiles for covalent inhibition pathways, and in this sense they might putatively share features in common with other known STAT3 inhibitors, such as LY5[30] and BA-TPQ,[31] with structures consistent with electrophilic reactivity. Significant decomposition of **C188–9** was observed within 4 hours in aqueous buffer under air (Figure S1), and crude NMR investigations showed new peaks consistent with a iminoquinone. In one case, an iminoquinone intermediate **2b*** (Table 2) was stable enough to be isolated, characterized, and tested. This iminoquinone also demonstrated significant binding affinity in our SPR-based assay, suggesting that iminoquinone intermediates may contribute to at least some function in vivo.

To further probe these issues, we prepared a brief series of **C188–9** analogues with an explicit goal of improving lifetime in media. Although some structural changes abrogated binding, a few did show promising binding by SPR, including fluoro-ether **12b** and triflate **19** (Table 2). Interestingly, O-acylation of the naphthol hydroxyl group has a significant negative effect on binding in the case of **17**, but substitution on oxygen is tolerated in other cases (e.g. **12b**, **18**, and **19**). Unlike the parent **C-188–9,** fluoro-ether **12b** and triflate **19** are indefinitely stable in aqueous buffer in air. The binding potency of **12b** and **19** suggests that oxidation and/or accessing an iminoquinone structure is not required for binding or activity.

Inhibition of intracellular phosphorylation

The more promising molecules (**3aa-3ca**) were tested in intracellular STAT3 phosphorylation assays. To extrapolate intracellular potency, Kasumi-1 human AML cells were treated with differing concentrations of inhibitor (Figure 3a). Cells were incubated with granulocyte-colony stimulating factor (G-CSF) to induce STAT3 phosphorylation.[32] After incubation, the cells were lysed and levels of STAT3 phosphorylated on tyrosine 705 (pSTAT3) were quantified with a fluorescent pSTAT3 antibody. Although **3aa**, **3ba**, and **3ca** performed similarly by SPR (Table 2), their ability to inhibit STAT3 phosphorylation in cells was markedly different. This suggests that their molecular recognition of STAT3 in an isolated system like SPR is similar, however, in a protein-rich redox-buffered environment these inhibitors no longer behave the same. It is important to note that differences in small molecule specificity and cellular uptake can also affect the intracellular potency of the inhibitors. Nevertheless, **3aa** was clearly the most potent small-molecule pSTAT3 inhibitor.

We wanted to ensure that the molecule **3aa** also inhibits inducible STAT3 phosphorylation in other AML cell lines (Figure 3b). Following a 30-minute treatment with **3aa** prior to G-CSF stimulation, all three of the AML cell lines tested (HL-60, MOLM-13, and Kasumi-1) exhibited dose-dependent decreases in STAT3 phosphorylation with IC_{50} 0.8–1.9 μM. This demonstrates that the anti-pSTAT3 activity of **3aa** can be seen across different AML cell lines.

To further evaluate the therapeutic potential of **3aa**, we confirmed its ability to induce apoptosis in different AML cell lines and primary tumor cells from pediatric AML patients. Cells were incubated with different doses of each inhibitor and subsequently incubated with fluorescent Annexin V. Annexin V binds to apoptotic cells, and FITC-Annexin V conjugates allow quantification of apoptosis by fluorescence assisted cell sorting (FACS). A 24-hour

treatment with **3aa** increased apoptosis in all AML cell lines and primary samples tested (Figure 3c). In contrast, acute lymphoblastic leukemia (ALL) cell lines—which do not have upregulated STAT3 activity[33]—were much less sensitive to apoptosis induction (Figure 3c, KOPN-8 and RS4–11). These findings are is consistent with the idea that **3aa** inhibits STAT3 phosphorylation in AML cell lines and induces apoptosis through that mechanism of action.

After thoroughly investigating our **3aa** in the *in vitro* models, we moved to investigate its potency in *in vivo* mouse models. STAT3-dependent cyctotoxicity in apoptosis assays suggested at least a half-log dosing window. Mice were injected intravenously with MV4–11 human AML cells. After two weeks, mice were treated for another 2–4 weeks with **3aa**. Results from *in vivo* imaging, bone marrow and spleen harvesting indicate that **3aa** increases mouse survival by decreasing the expansion of MV4–11 leukemia cells (Figure 3 d–f).

Rhodium conjugates as STAT3 inhibitors

After garnishing some promising results in the traditional small molecule studies with **3aa**, we shifted our focus to the biological efficacy of small molecule-rhodium conjugates. Again, we used SPR to screen inhibitor potency (Table 3). Rhodium-inhibitor conjugate **13aa**, **13ac**, and **13b**, showed potency increases over their analogous esters. Compared to previous studies with other binding sites, this affinity gain is rather modest, and is presumably consistent with at most very weak binding to side chains such as carboxylates (i.e. residue Asp 170 near the coiled-coil binding site) rather than stronger binding to histidine or methionine. A previous study found that sterically demanding carboxylates improved the decomposition half-life of rhodium complexes,[34] but the sterically crowded rhodium complex **13ac** had potency similar to other rhodium conjugates. The divalent structure **13ad** did demonstrate moderately improved STAT3 affinity (0.1 μM).

It seemed possible that a more Lewis-acidic rhodium center could benefit from more potent binding to peripheral residues.[35] The coiled-coil domain does have several carboxylate side chains near the ligand-binding site (Figure 1a, **blue**), including Asp170, and we reasoned that carboxylates, while weaker ligands than histidine or methionine, might be sufficient ligands for a metal center with increased Lewis acidity. Alteration of the ancillary ligands on rhodium allows tuning the Lewis acidity of the metal center. An electron-poor variant, **13ae** did show improved binding to STAT3 (IC_{50} = 0.04 μM, Table 3): compound **13ae** is 100× more potent than C188–9, and 25× more potent than the nearly isosteric rhodium complex **13aa**. This effect may be quite subtle: The analogous *tris*-trifluoroacetate complex (**13af**) exhibited a more modest affinity enhancement (IC_{50} = 0.2 μM, Table 3), perhaps reflecting a subtle balance of competitive water binding.[34]

Next, we examined the cellular activity of the lead rhodium conjugate on STAT3 phosphorylation and the induction of apoptosis in Kasumi cells (Figure 4). To provide a useful comparison, rhodium conjugates were directly compared against C188–9 and compound 4a, an isoelectric organic analogue without the capacity for coorperative organic–inorganic binding. In STAT3 intracellular phosphorylation assays (Figure 4b), the electronically-perturbed rhodium complex **13ae** again exhibited significantly improved

activity. The Kasumi cells were exceptionally resistant to both C188–9 and 4a, while 13ae inhibited STAT3 phosphorylation at lower micromolar potencies. In all, this is the first example of rhodium complexation enhancing the potency of any intracellular inhibitor in cellular assays andthese results indicate that rhodium conjugation is a viable strategy for increasing the potency of a biological probe for intracellular assays.

In order to see if this increase phosphorylation inhibition translated to induction of apoptosis, we compared **13ae**, **4a**, and **C188–9** in an Annexin assay (Figure 4c). The rhodium complex **13ae** was more potent than both **C188–9** and **4a,** which is in agreement with the phosphorylation inhibition results. Therefore the fact that **13ae** consistently outperformed C188–9 in these in vitro assays suggests further development of rhodium conjugates is warranted.

Naphthalene sulfonamides are a useful class of probes to alter STAT3 function. Optimization of the sulfonamide core allowed development of **3aa**, an inhibitor with improved binding potency, and anti-STAT3 activity in cells. Some of the naphthalene sulfonamides also display *in vivo* activity in relevant cancer models.[11,36] For example, pentafluoro compound **3aa**, significantly decreases tumor progression in a mouse model of AML. Anti-phosphorylation activity correlates well with apoptosis induction in tumor models for the naphthalene sulfonamide compound class, again consistent with a specific STAT3-driven mode of action. Overall, optimization of the naphthalene sulfonamide core has resulted in modest gains in potency and activity, perhaps due to innate features of the coiled-coil binding site, which lacks a deep ligand-binding pocket. This limited optimization success led us to pursue tandem efforts to explore rhodium conjugates as potential solution to vexing inhibitor-development problems. The substantial increase in potency observed with rhodium complex **13ae** indicates that significant gains in binding affinity are possible, even without proximal strong metal-binding residues (histidine, methionine, cysteine), by perturbing the electronic structure of the rhodium center in favor of increased Lewis acidity. Perhaps most importantly, the improvement in STAT3 binding carries through to cell-based assays, supporting our previous conclusions that rhodium complexes can enter and act within living cells. Complexes such as **13ae** may serve as probe compounds with unique specificity; although many important questions remain, especially regarding *in vivo* application of these compounds.

Supplementary Material

Refer to Web version on PubMed Central for supplementary material.

Acknowledgements

References

1. Bromberg J, J. Clin. Invest, 2002, 109, 1139–1142. [PubMed: 11994401]

2. Darnell JE, Kerr IM and Stark GR, Science, 1994, 264, 1415–1421. [PubMed: 8197455]

3. Kisseleva T, Bhattacharya S, Braunstein J and Schindler CW, Gene, 2002, 285, 1–24. [PubMed: 12039028]

4. Chakraborty A, Dyer KF, Cascio M, Mietzner TA and Tweardy DJ, Blood, 1999, 93, 15–24. [PubMed: 9864141]

5. Wu P, Wu D, Zhao L, Huang L, Shen G, Huang J and Chai Y, Oncotarget, 2016, 7, 19863–19883. [PubMed: 26959884]

6. Kamran MZ, Patil P and Gude RP, BioMed Res. Int,, DOI:10.1155/2013/421821.

7. Johnson DE, O'Keefe RA and Grandis JR, Nat. Rev. Clin. Oncol, 2018, 15, 234–248. [PubMed: 29405201]

8. Zhang X, Yue P, Page BDG, Li T, Zhao W, Namanja AT, Paladino D, Zhao J, Chen Y, Gunning PT and Turkson J, Proc. Natl. Acad. Sci, 2012, 109, 9623–9628. [PubMed: 22623533]

9. Chen Y, Ji M, Zhang S, Xue N, Xu H, Lin S and Chen X, J. Drug Target, 2018, 26, 920–930. [PubMed: 29595328]

10. Geiger JL, Grandis JR and Bauman JE, Oral Oncol, 2016, 56, 84–92. [PubMed: 26733183]

11. Bharadwaj U, Eckols TK, Xu X, Kasembeli MM, Chen Y, Adachi M, Song Y, Mo Q, Lai SY and Tweardy DJ, Oncotarget, 2016, 7, 26307–26330. [PubMed: 27027445]

12. Park JH, van Wyk H, McMillan DC, Quinn J, Clark J, Roxburgh CSD, Horgan PG and Edwards J, Clin. Cancer Res, 2017, 23, 1698–1709. [PubMed: 27678454]

13. He G and Karin M, Cell Res, 2011, 21, 159–168. [PubMed: 21187858]

14. Redell MS, Ruiz MJ, Alonzo TA, Gerbing RB and Tweardy DJ, Blood, 2011, 117, 5701–9. [PubMed: 21447830]

15. Minus MB, Liu W, Vohidov F, Kasembeli MM, Long X, Krueger M, Stevens A, Kolosov MI, Tweardy DJ, Redell MS and Ball ZT, Angew. Chem. Int. Ed, 2015, 54, 13085–13089.

16. Abdulghani J, Gu L, Dagvadorj A, Lutz J, Leiby B, Bonuccelli G, Lisanti MP, Zellweger T, Alanen K, Mirtti T, Visakorpi T, Bubendorf L and Nevalainen MT, Am. J. Pathol, 2008, 172, 1717–1728. [PubMed: 18483213]

17. Yu H, Lee H, Herrmann A, Buettner R and Jove R, Nat. Rev. Cancer, 2014, 14, 736–746. [PubMed: 25342631]

18. Johnston PA and Grandis JR, Mol. Interv, 2011, 11, 18–26. [PubMed: 21441118]

19. Dang CV, Reddy EP, Shokat KM and Soucek L, Nat. Rev. Cancer, 2017, 17, 502–508. [PubMed: 28643779]

20. Verdine GL and Walensky LD, Clin. Cancer Res, 2007, 13, 7264–7270. [PubMed: 18094406]

21. Xu X, Kasembeli MM, Jiang X, Tweardy BJ and Tweardy DJ, PLoS ONE, 2009, 4, e4783. [PubMed: 19274102]

22. Ren Z, Mao X, Mertens C, Krishnaraj R, Qin J, Mandal PK, Romanowski MJ, McMurray JS and Chen X, Biochem. Biophys. Res. Commun, 2008, 374, 1–5. [PubMed: 18433722]

23. Kundu R, Cushing PR, Popp BV, Zhao Y, Madden DR and Ball ZT, Angew. Chem. Int. Ed, 2012, 51, 7217–7220.

24. Vohidov F, Knudsen SE, Leonard PG, Ohata J, Wheadon MJ, Popp BV, Ladbury JE and Ball ZT, Chem. Sci, 2015, 6, 4778–4783. [PubMed: 29142714]

25. Ma H, Wu S, Sun Q, Li H, Chen Y, Zhao W, Ma B, Guo Q, Lei Z and Yan J, Synthesis, 2010, 2010, 3295–3300.

26. Mallory FB, Mallory CW and Fedarko MC, J. Am. Chem. Soc, 1974, 96, 3536–3542.

27. Schimler SD, Ryan SJ, Bland DC, Anderson JE and Sanford MS, J. Org. Chem, 2015, 80, 12137–12145. [PubMed: 26647642]

28. Popp BV and Ball ZT, J. Am. Chem. Soc, 2010, 132, 6660–6662. [PubMed: 20420453]

29. Page BDG, Fletcher S, Yue P, Li Z, Zhang X, Sharmeen S, Datti A, Wrana JL, Trudel S, Schimmer AD, Turkson J and Gunning PT, Bioorg. Med. Chem. Lett, 2011, 21, 5605–5609. [PubMed: 21788134]

30. Zhao C, Wang W, Yu W, Jou D, Wang Y, Ma H, Xiao H, Qin H, Zhang C, Lü J, Li S, Li C, Lin J and Lin L, Oncotarget, 2016, 7, 12917–12926. [PubMed: 26883202]

31. Wang W, Rayburn ER, Velu SE, Chen D, Nadkarni DH, Murugesan S, Chen D and Zhang R, Breast Cancer Res. Treat, 2010, 123, 321–331. [PubMed: 19936915]

32. Shimozaki K, Nakajima K, Hirano T and Nagata S, J. Biol. Chem, 1997, 272, 25184–25189. [PubMed: 9312131]

33. Furuichi Y, Goi K, Inukai T, Sato H, Nemoto A, Takahashi K, Akahane K, Hirose K, Honna H, Kuroda I, Zhang X, Kagami K, Hayashi Y, Harigaya K, Nakazawa S and Sugita K, Cancer Res, 2007, 67, 9852–9861. [PubMed: 17942916]

34. Minus MB, Kang MK, Knudsen SE, Liu W, Krueger MJ, Smith ML, Redell MS and Ball ZT, Chem. Commun, 2016, 52, 11685–11688.

35. Coughlin JM, Kundu R, Cooper JC and Ball ZT, Bioorg. Med. Chem. Lett, 2014, 24, 5203–5206. [PubMed: 25442313]

36. Jung KH, Yoo W, Stevenson HL, Deshpande D, Shen H, Gagea M, Yoo S-Y, Wang J, Eckols TK, Bharadwaj U, Tweardy DJ and Beretta L, Clin. Cancer Res, 2017, clincanres.2253.2016.
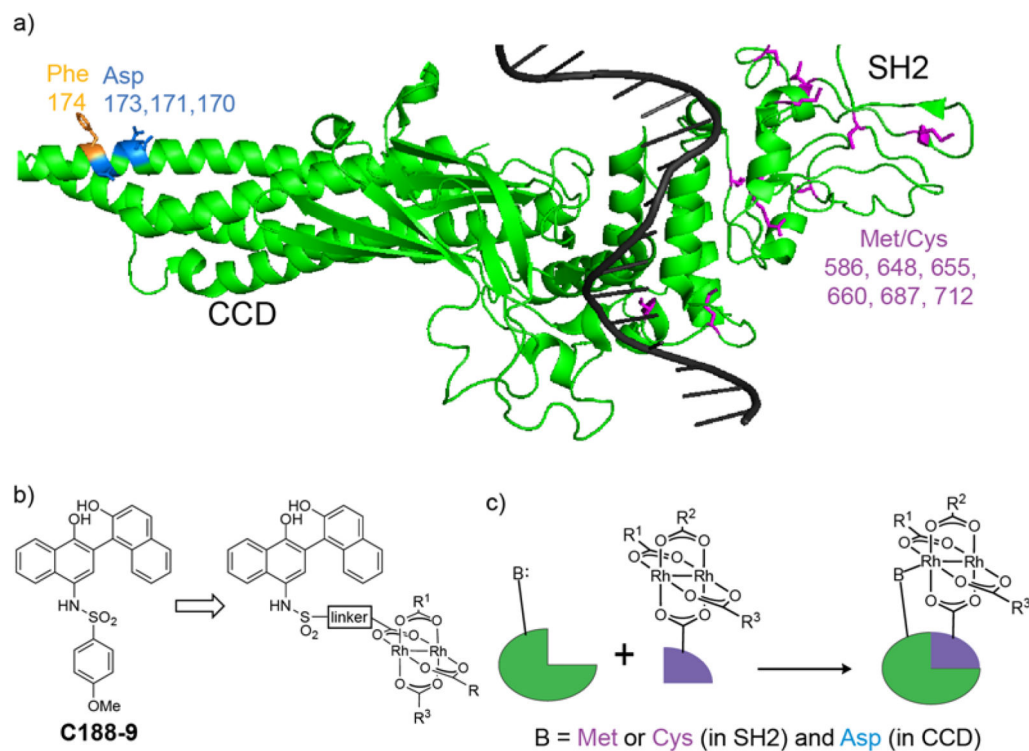
Figure 1.
(a) Crystal structure of a single STAT3 protein when bound as a dimer to duplex DNA.[22] Nucleophilic ligands, cysteine and methionine residues of the SH2 domain (purple) and aspartate ligands of the coiled-coil domain (blue) are highlighted. Affinity labeling experiments with a rhodium inhibitor conjugate indicates that binding occurs at/near Phe174 (orange) in the coiled-coil domain. (b) A lead compound, C188–9 (a.k.a. TTI-101). (c) Rh-STAT3 conjugates use inorganic-organic cooperativity to bind STAT3.
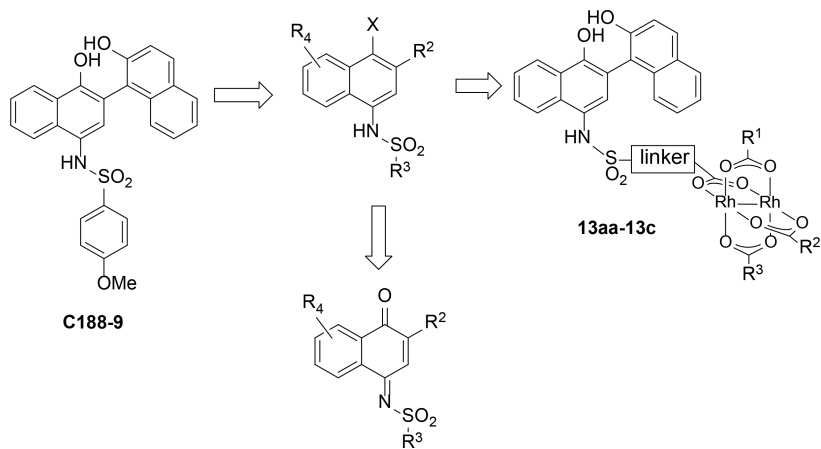
Figure 2.
Previously established STAT3 inhibitor motif,[21] and expanded motifs discovered in this work.
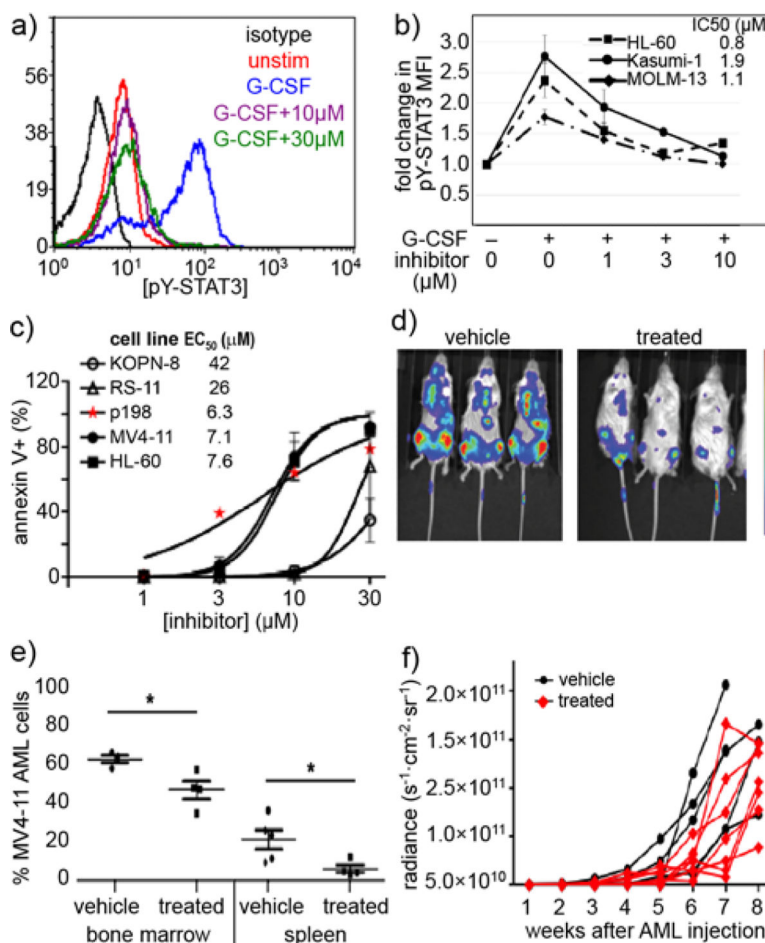
Figure 3.
Portions of this figure were adapted from a preliminary report.[15] Compound **3aa** inhibits G-CSF-induced STAT3 phosphorylation, induces apoptosis in human AML cells, and slows disease progression in a xenograft model of AML. (a) Histogram of decrease in pSTAT3 in Kasumi-1 cells. (b) 10 inhibits G-CSF-induced pSTAT3 in multiple AML cell lines. Legend values indicate IC_{50} values. Mean ±SD for n = 3. (c) Apoptosis quantified in Annexin V-FITC-labeled cells treated with 10 for 24 h. Spontaneous apoptosis in untreated cells was subtracted to yield the % apoptosis attributable to drug. Data shown for an AML cell line (MV4–11, HL-60) and primary patient-derived AML cells (p198) compared to ALL cell lines (KOPN-8, RS4–11) as a negative control. (d-e) NSG mice were injected iv with 10^6 MV4–11. ffluc AML cells at day 0. After two weeks, mice received compound 10, 30 mg/kg (n=8), or vehicle (n=6), ip daily 5 d/week for 4 weeks (weeks 2–6). (d) Luminescence images one week after treatment. Colorized signal intensity indicates amount of active disease, from low (blue) to high (red). (e) The percent of MV4–11 cells in bone marrow and spleen was evaluated by flow cytometry at the time of euthanasia. *P<0.05 (f) Disease burden was measured non-invasively by bioluminescence weekly. Each line represents the trajectory of an individual mouse. Mice were euthanized when moribund or at the end of 8 weeks.
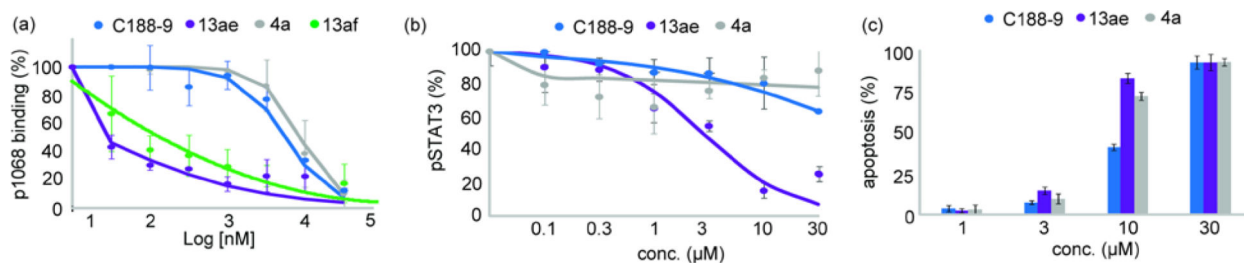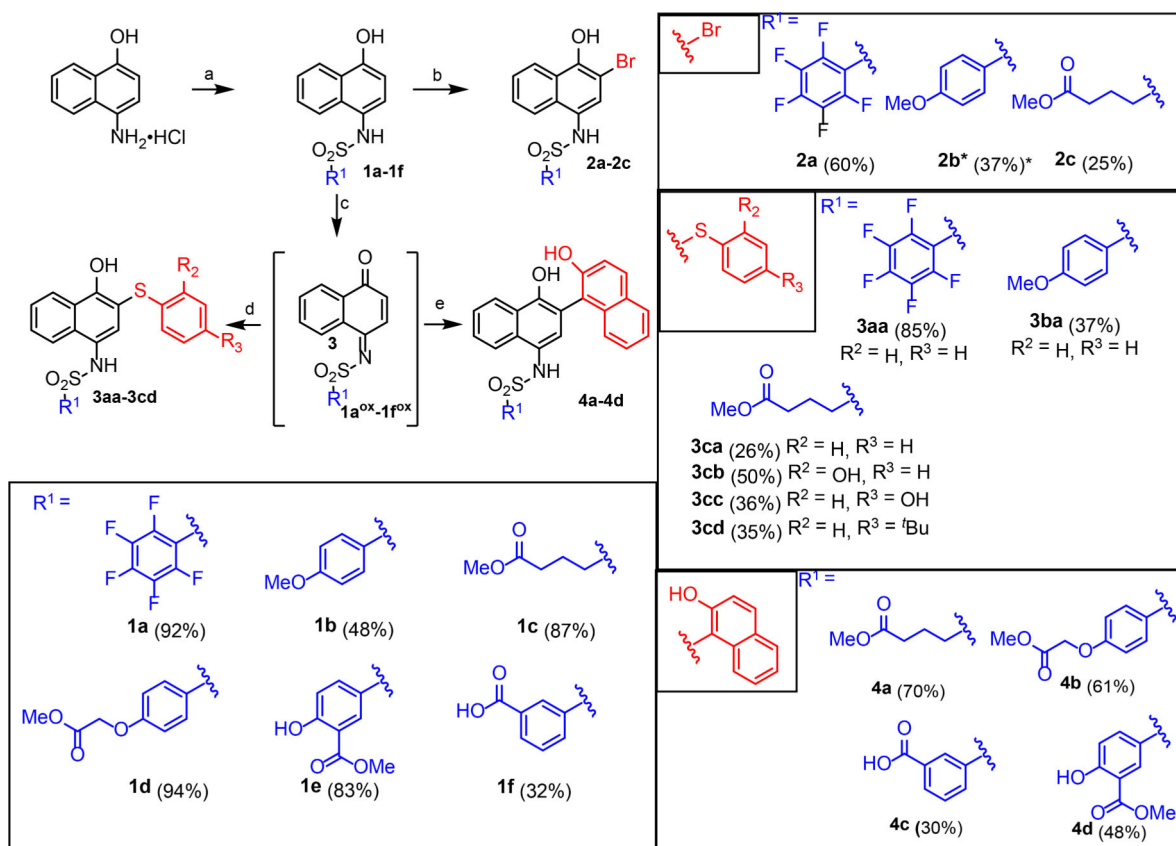
Figure 4.
(a) Small molecules inhibit STAT3/phosphopeptide (p1068) binding. STAT3 phosphopeptide binding was measured with established SPR protocols.21 (b) Kasumi cells were treated with G-CSF and then with inhibitors. Cells were analyzed for phosphorylated STAT3 (pSTAT3). (c) Apoptosis was measured 24 h after treatment of AML cells with STAT3 inhibitors.

Scheme 1.

Modular synthesis of STAT3 inhibitors (a) R^1SO_2Cl, pyridine, MeCN, $MgSO_4$ (32–94%) (b) Br_2, CH_2Cl_2 (25–60%) (c) $PhI(OAc)_2$, acetone (d) PhSH, HCOOH (26–85%) (e) $BF_3 \cdot Et_2O$, 2-naphthol (30–70%). Yields for oxidative coupling were taken over 2 steps. (*) Inhibitor isolated as oxidized iminonaphthoquinone.
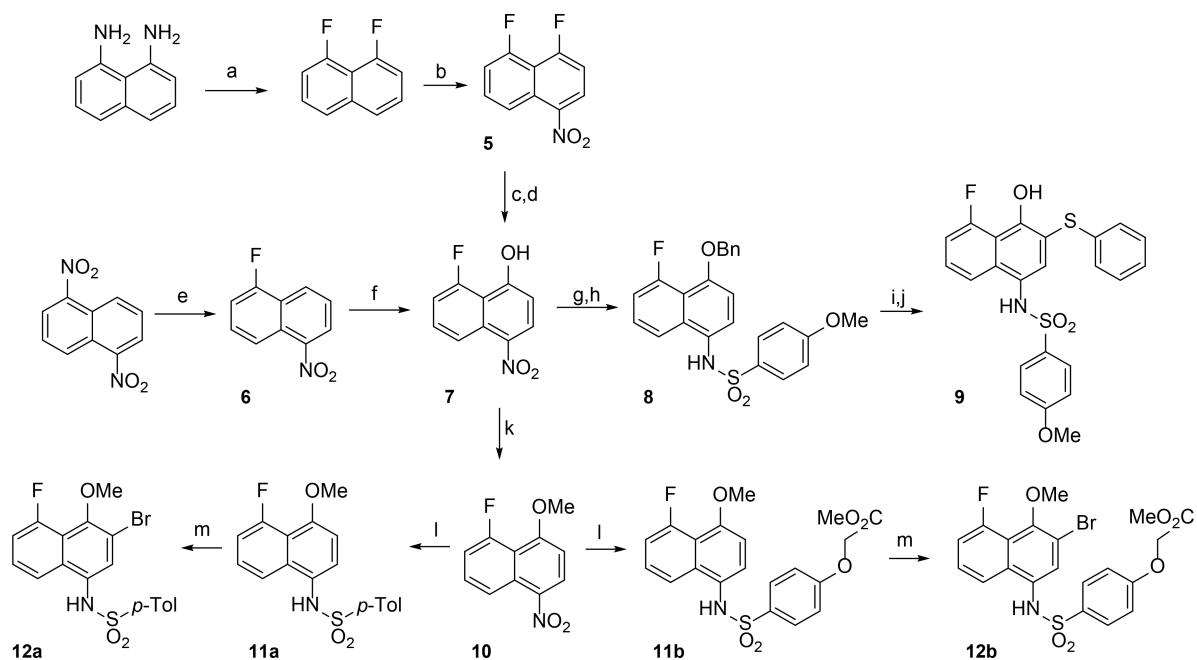
Scheme 2.

Synthesis of 5-fluoronaphthylsulfonamides (a) i) HBF$_4$ (aq) NaNO$_2$ ii) molten KHF$_2$ (2–20%) (b) HNO$_3$, NaNO$_2$ (60%) (c) BnOH, NaH, CH$_2$Cl$_2$ (61%) (d) Pt/C, NaBH$_4$ (99%) (e) CsF, DMSO, 100 °C (23%) (f) NH$_3$, TBHP, NaOH, THF (70%) (g) BnBr, Cs$_2$CO$_3$, CH$_2$Cl$_2$ (75%) (h) i) Pt/C, NaBH$_4$ ii) 4-methoxybenzenesulfonyl chloride, pyridine, MgSO$_4$ (62%) (i) Pd/C, H$_2$, (j) PhI(OAc)$_2$, PhSH, (CF$_3$)$_2$CHOH (37%) (k) MeI, K$_2$CO$_3$, DMF (84%) (l) i) Pd/C, NaBH$_4$ ii) R$_2$SO$_2$Cl, pyridine, MgSO$_4$ (45–89%) (m) Br$_2$, CH$_2$Cl$_2$ (56–75%)

Table 1.

Preparation of rhodium conjugates by carboxylate exchange with heteroleptic rhodium trifluoroacetates.
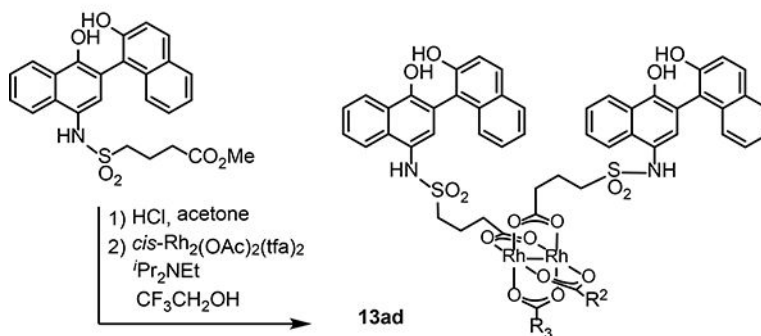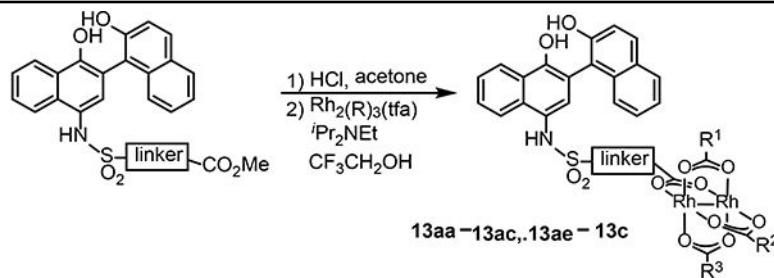
entry	linker	product	R_1	R_2	R_3	yield (%)
1	4a	13aa	Me	Me	Me	63
2		13ab	^nBu	^nBu	^nBu	15
3		13ac	fluorescein	Me	Me	21
4		13ad	n.a.	Me	Me	15
5		13ae	CF_3	Me	Me	42
6		13af	CF_3	CF_3	CF_3	15
7	4b	13b	Me	Me	Me	37
8	4c	13c	Me	Me	Me	8

Table 2.

Inhibition of STAT3 phosphopeptide binding. Inhibitive potency (IC$_{50}$) was determined by established SPR and/or a cellular STAT3 phosphorylation assay.

Table 3.

SPR analysis of binding for carboxylate-containing and rhodium-conjugate compounds.

					SPR IC_{50} (uM)	
entry	cmpd	R_1	R_2	R_3	ester	Rh(II)
1	**13aa**	Me	Me	Me	25	1
2	**13ab**	^{n}Bu	^{n}Bu	^{n}Bu	25	0.6
3	**13ac**	fluorescein	Me	Me	25	1
4	**13ad**	**n.a.**	Me	Me	25	0.1
5	**13ae**	CF_3	Me	Me	25	0.04
6	**13af**	CF_3	CF_3	CF_3	25	0.2
7	**13b**	Me	Me	Me	8	1
8	**13c**	Me	Me	Me	50^*	0.3

[*] SPR IC_{50} of the carboxylic acid derivative **4c** was measured.